ACS Catalysis

Research Article

pubs.acs.org/acscatalysis

Isokinetic Temperature and Size-Controlled Activation of Ruthenium-Catalyzed Ammonia Borane Hydrolysis

Hanyu Ma and Chongzheng Na*

Department of Civil and Environmental Engineering and Earth Sciences, University of Notre Dame, Notre Dame, Indiana 46556, United States

Supporting Information

ABSTRACT: Metal-catalyzed hydrolysis is an important reaction for releasing hydrogen stored in ammonia borane, a promising fuel form for the future hydrogen economy, under ambient conditions. A variety of catalysts made of different transition metals have been investigated to improve the efficiency of hydrogen generation; however, little attention has been given to the possible influence of the compensation effect on catalyst design. Using face-centered cubic (FCC) packed ruthenium (Ru) nanoparticles supported on layered double oxide nanodisks, we show that the compensation effect produces an isokinetic temperature at T_i = 17.5(±1.6) °C within the operational range of hydrogen generation. We further show that the turnover frequency (TOF) of the reaction can be maximized for operations performed below T_i by reducing the size of Ru-FCC nanoparticles, which increases the fraction of edge and corner atoms and lowers the activation energy. At 15 °C, TOF can reach more than 90% of the theoretical maximum (0.72 mol m^{-2} h^{-1}) using Ru nanoparticles having an average diameter of 2 nm and giving an activation energy of 17.7(±0.7) kJ mol^{-1}. To generate hydrogen above T_i, TOF is maximized by using enlarged Ru nanoparticles with a diameter of 3.8 nm, giving an activation energy of 87.3(±5.8) kJ mol^{-1}. At 25 °C, these nanoparticles produce a TOF of 1.8(±0.3) mol m^{-2} h^{-1}, representing at least an 81% increase in comparison to the highest TOF reported for elemental catalysts. Our results suggest that controlling the reaction activation energy by adjusting nanoparticle size represents a viable strategy for designing catalysts that can maximize TOF for ammonia borane hydrolysis operated both below and above the isokinetic temperature.

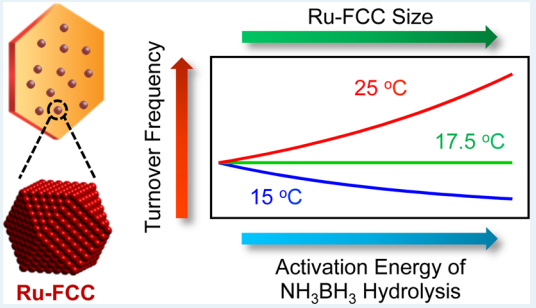

KEYWORDS: *compensation effect, isokinetic temperature, metal hydride, hydrogen storage and production, nanoparticle nucleation, supported and stabilized nanocatalyst, layered double hydroxide derivative*

INTRODUCTION

A main objective of heterogeneous catalysis is to improve reaction kinetics by adjusting the reaction activation energy E_a through catalyst design.[1,2] When the turnover frequency (TOF) of the reaction becomes insensitive to the adjustment, the temperature under which the insensitivity incurs is referred to as the isokinetic temperature T_i. T_i originates from the compensation effect,[3−5] which manifests in a linear correlation between E_a and the natural logarithm of the Arrhenius pre-exponential factor A (aka the Cremer−Constable relation):[5,6]

$$\ln A = \alpha E_a + \beta \tag{1}$$

where α and β are constants. E_a and A are related to TOF by the Arrhenius equation for zeroth-order reactions:[7,8]

$$\mathrm{TOF} = A \exp\left(-\frac{E_a}{RT}\right) \tag{2}$$

where R is the gas constant and T is the absolute temperature. Combining eqs 1 and 2 gives

$$\mathrm{TOF} = \mathrm{TOF}_i \exp\left[-\frac{E_a}{R}\left(\frac{1}{T} - \frac{1}{T_i}\right)\right] \tag{3}$$

with $T_i = \alpha^{-1}R^{-1}$ and $\mathrm{TOF}_i = e^{\beta}$ for $T = T_i$. For reactions showing the compensation effect, estimates of T_i almost exclusively lie outside the operational range of T,[6,9] giving scenarios of either $T < T_i$ or $T > T_i$. To maximize TOF, catalysts should be designed to decrease E_a if $T < T_i$ but increase E_a if $T > T_i$. Only a few exceptions such as the catalytic synthesis of ammonia have T_i within the operational range of T.[6] Under such conditions, the influence of E_a on TOF depends on the relative magnitudes of T and T_i.

Ammonia borane (NH_3BH_3) is a safe and efficient form for storing hydrogen to power vehicles and portable devices.[10−15] Hydrogen can be released from ammonia borane as the H_2 gas through metal-catalyzed hydrolysis under ambient conditions:[16]

Received: December 5, 2014
Revised: January 11, 2015
Published: January 30, 2015

DOI: 10.1021/cs5019524
ACS Catal. 2015, 5, 1726−1735

$$NH_3BH_3 + 2H_2O \xrightarrow{\text{catalyst}} NH_4^+ + BO_2^- + 3H_2 \quad (4)$$

Given the urgency of replacing fossil fuels with clean and renewable energy sources such as hydrogen, it is not surprising that a wide variety of catalysts made of ruthenium (Ru),[16−27] platinum (Pt),[28,29] palladium (Pd),[18,30−33] nickel (Ni),[34−36] cobalt (Co),[37−40] iron (Fe),[41] and their alloys[42−46] have been investigated to improve the efficiency of ammonia borane hydrolysis. Surprisingly, however, little attention has been given to the possible influence of the compensation effect and thus the existence of an isokinetic temperature on catalyst design. After compiling experimental values of A and E_a from 26 reports,[16−41] as shown in Figure 1a (cf. Table S1 in the Supporting Information), we have observed a linear correlation between ln A and E_a, strongly suggesting the influence of the compensation effect on the kinetics of ammonia borane hydrolysis. Least-squares regression to eq 3 gives an isokinetic temperature of T_i = 293(±11) K = 20(±11) °C, comparable to the operational temperatures of ammonia borane hydrolysis under ambient conditions. As a result, the maximization of TOF requires the ability to design and fabricate catalysts that can both minimize and maximize E_a depending on whether hydrolysis is operated at $T < T_i$ or $T > T_i$.

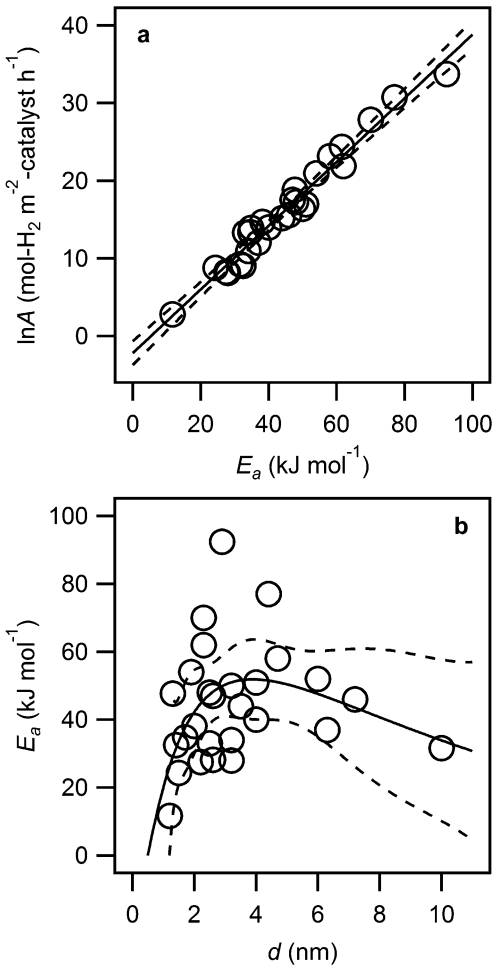

Figure 1. Performance of transition-metal nanoparticles in catalytic ammonia borane hydrolysis: (a) correlation between the Arrhenius pre-exponential factor A and the activation energy E_a; (b) correlation between E_a and the particle diameter d. Solid curves are least-squares regressions (a, linear with R^2 = 0.97; b, log-normal). Dashed curves bracket 95% confidence bands. Nanoparticles included in this figure are made of ruthenium, platinum, palladium, nickel, cobalt, and iron (see Table S1 in the Supporting Information for data and sources).

A few recent studies have shown that the activation energy of a heterogeneous catalytic reaction can be controlled by varying the size of catalyst nanoparticles.[47] In the nanometer range, the decrease of particle size often leads to an increase in the fraction of edge and corner atoms, which can stabilize reaction intermediates better than atoms located on a flat terrace. Consequently, the decrease of nanoparticle size can lower the reaction activation energy. Likewise, the activation energy can be increased by using large catalyst nanoparticles. The effect of catalyst size on E_a has been observed for Pd-catalyzed p-nitrophenol reduction and Pt-catalyzed ethane hydrogenolysis and cyclohexene dehydrogenation.[47−49] Although there has not been a systematic study of the size effect for ammonia borane hydrolysis, data compiled from the literature[16−41] shown in Figure 1b suggests that a positive and monotonic correlation likely exists between E_a and the nanoparticle diameter d for d < 4 nm.

Here, we report the synthesis and evaluation of face-centered cubic (FCC) packed Ru nanoparticles with diameters between 2 and 3.8 nm, which have tunable activation energies from 18 to 87 kJ mol^{-1} in ammonia borane hydrolysis. Using Ru-FCC, we show that ammonia borane hydrolysis has an isokinetic temperature of T_i = 17.5(±1.6) °C, comparable to the value estimated from literature data but with much reduced uncertainty. More importantly, we show that at 15 °C (i.e., $T < T_i$) the TOF of hydrogen production can reach more than 90% of the expected maximum of TOF_i = 0.72 mol m^{-2} h^{-1} using 2.0 nm Ru-FCC nanoparticles. At 25 °C (i.e., $T > T_i$), 3.8 nm Ru-FCC gives a TOF of 1.8 mol m^{-2} h^{-1}. This represents an 81% increase from the highest TOF reported so far for ruthenium, the most effective elemental catalyst for ammonia borane hydrolysis.[16,20,50]

RESULTS

Ru-FCC nanoparticles are prepared on two-dimensional layered double oxide (LDO) support using a two-step method as illustrated in Figure 2a. First, LDO nanodisks are immersed in an aqueous solution containing ruthenium chloride ($RuCl_3$) for 24 h. LDO nanodisks, prepared by us in this study, have a polycrystalline spinel ($MgAl_2O_4$) structure and a pseudo-two-dimensional hexagonal shape,[51] as shown in Figure 2b,c. The hexagons have a nominal diameter of ca. 4 μm but a thickness of only 40 nm. The ultrahigh surface-to-volume ratio of LDO nanodisks maximizes their potential as catalyst support.[52] Second, after being washed with deionized (DI) water, LDO nanodisks are immersed in an aqueous solution saturated with ammonia borane, reducing Ru^{3+} adsorbed on the nanodisk surface to Ru^0 nanoparticles. Transmission electron microscopy (TEM), shown in Figures 2d,e, confirms that Ru nanoparticles formed by reduction are well dispersed on the LDO surface.

High-resolution TEM reveals that Ru nanoparticles are FCC single crystals with a diameter between 2 and 3.8 nm, as shown in Figure 3a. The FCC structure is confirmed by fast Fourier transform (FFT) of the micrograph, as shown in Figure 3b, giving an electron diffraction pattern consistent with an FCC crystal viewed along the [110] zone axis.[53,54] The diffraction spots are formed by the reflections of {111} and {002} planes, giving a lattice constant of 0.371(±0.004) nm, consistent with a theoretical value of 0.375 nm for Ru-FCC.[54,55] The FCC structure, together with the hexagonal shape in the TEM image,

DOI: 10.1021/cs5019524
ACS Catal. 2015, 5, 1726−1735

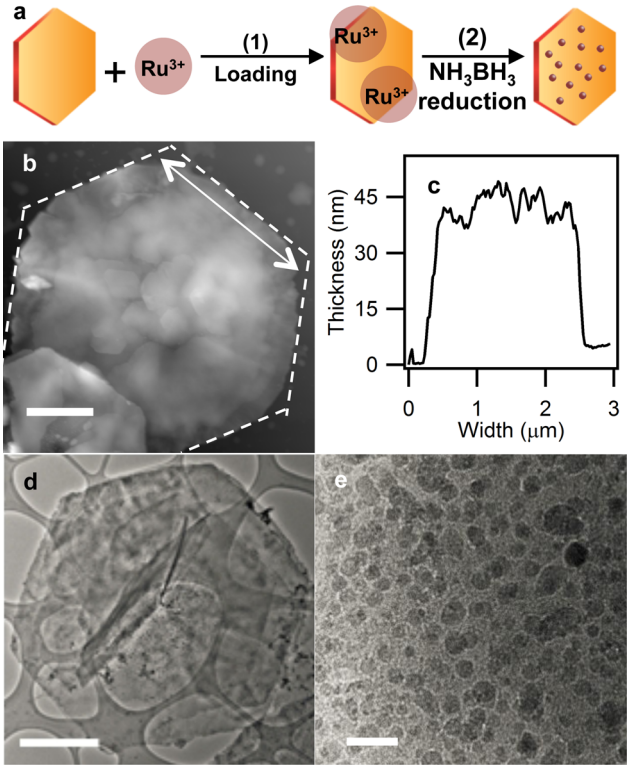

Figure 2. Preparation and morphology of Ru-FCC nanoparticles supported on layered double oxide (LDO) nanodisks: (a) major steps in preparation; (b) atomic force micrograph (AFM) of LDO nanodisks; (c) AFM profile (location marked by the double-arrow line in (b)) showing the thickness of LDO nanodisks; (d) transmission electron micrograph (TEM) of LDO-Ru-FCC; (e) TEM of Ru nanoparticles on LDO. Scale bars: (b) and (d), 1 μm; (e), 10 nm.

further suggests that a Ru nanoparticle is a truncated octahedron when standing alone, having eight {111} and six {100} facets.[56] The lattice structure of Ru-FCC can be viewed as the alternating stacking of three different {111} layers of closely packed atoms, as shown by different colors in Figure 3c.

To compare with Ru-FCC, adding both LDO and ammonia borane into the $RuCl_3$ solution simultaneously produces hexagonal close packed (HCP) Ru nanoparticles. The addition of NH_3BH_3 immediately reduces Ru^{3+} in solution to Ru^0 nanoparticles, which then adhere to LDO surfaces. As shown in Figure 3d,e, Ru-HCP nanoparticles are also single crystals but have a different electron diffraction pattern. Ru-HCP is constructed by the alternating stacking of two different {001} layers of closely packed atoms, as shown in Figure 3f.

When LDO-Ru-FCC is used to catalyze hydrogen generation from the hydrolysis of NH_3BH_3 at a concentration of 100 mM, we find that the gas product is H_2 of high purity, with only 95(±12) ppm of ammonia as detected by colorimetric titration. The minimal amount of ammonia release indicates that most of the ammonium cation produced by reaction 4 stays in the aqueous solution. This is consistent with the formation of boric acid (H_3BO_3) from BO_2^- and H^+ and the subsequent increase of pH under our experimental conditions.[57] For analytical purposes, hydrogen generated by hydrolysis can be measured by the total volume of the gas because of its high purity. The volume of H_2 is then converted to the number of moles using the molar volume of an ideal gas at 25 °C (i.e., 24.5 mL $mmol^{-1}$), at which the buret used to collect the gaseous product is maintained. In practice, the trace amount of NH_3 can be readily removed from hydrogen before it is used to power hydrogen fuel cells.[58]

Figure 4a shows that the molar accumulation of hydrogen, n, released from LDO-Ru-FCC catalyzed NH_3BH_3 hydrolysis increases monotonically with time t. In comparison, LDO nanodisks containing no Ru nanoparticles cannot catalyze the reaction. The n–t plot for LDO-Ru-FCC reveals three kinetic regimes, including (I) a regime with increasing rates at $t < 5$ min, (II) a regime with a stabilized rate at $5 < t < 11$ min, and (III) a regime with decreasing rates at $t > 11$ min. We interpret regime I as the continuing reduction of Ru^{3+} to Ru^0 by

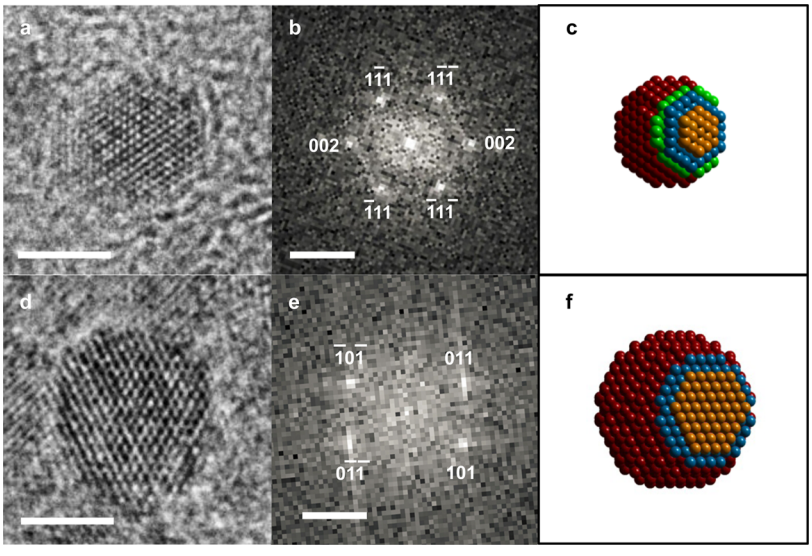

Figure 3. Structures of Ru-FCC and Ru-HCP nanoparticles supported on layered double oxide nanodisks: (a) high-resolution transmission electron micrograph (HRTEM) of Ru-FCC; (b) fast Fourier transform (FFT) of (a) (view direction: [110]); (c) truncated octahedral model for Ru-FCC with the top three layers of atoms of a (111) facet colored differently to illustrate the stacking of closely packed atoms in Ru-FCC; (d) HRTEM of Ru-HCP (view direction: [11$\bar{1}$]); (e) FFT of (d); (f) truncated octahedral model for Ru-HCP, with the top two layers of atoms of a (001) facet colored differently to illustrate the stacking of closely packed atoms in Ru-HCP. Scale bars: (a) and (d), 2 nm; (b) and (e), 5 nm^{-1}.

DOI: 10.1021/cs5019524
ACS Catal. 2015, 5, 1726–1735

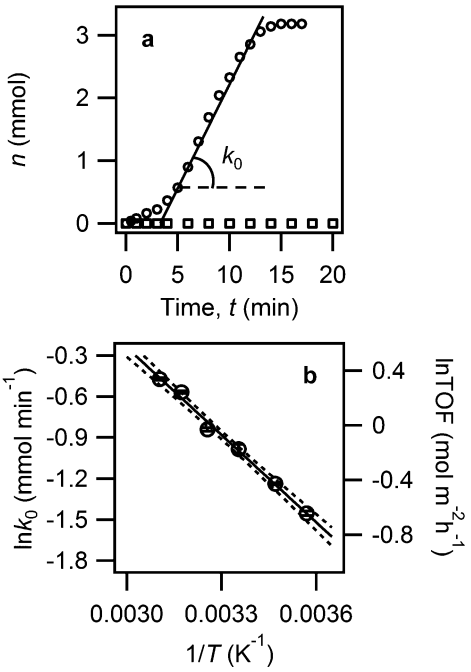

Figure 4. Evaluation of the catalytic performance of layered double oxide (LDO) supported Ru-FCC nanoparticles in ammonia borane hydrolysis: (a) accumulation of the number of moles of hydrogen generated by hydrolysis, n, over time t, which is used to estimate the pseudo-zeroth-order rate constant k_0; (b) correlation of k_0 and the turnover frequency (TOF) with temperature T according to the Arrhenius equation (eq 1). Solid curves are least-squares regressions ((a), linear; (b), eq 1). Dashed curves in (b) bracket 95% confidence bands. Error bars in (b) represent standard errors. Mean diameter of Ru-FCC nanoparticles: 2 nm.

NH_3BH_3, in which the reaction rate increases as an increasing amount of Ru^0 becomes available. Once all Ru^{3+} is reduced to the metallic state, the catalyst reaches its maximum potential, giving a stable reaction rate (i.e., regime II) until NH_3BH_3 becomes depleted (i.e., regime III). We estimate the catalytic activity of LDO-Ru-FCC by fitting the experimental data of regime II to the pseudo-zeroth-order rate law:

$$n = n_0 + k_0(t - t_0) \quad (5)$$

where n_0 and t_0 are the total moles of H_2 and time at the beginning of regime II, respectively, and k_0 is the rate constant. Linear regression gives k_0 = 0.35(±0.01) mmol-H_2 min^{-1} for the data presented in Figure 4a (see Table S2 in the Supporting Information for the selection of experimental data for regression).

We further compute the turnover frequency by dividing k_0 with the total surface area of Ru nanoparticles, τ:[59]

$$\mathrm{TOF} = \frac{k_0}{\tau} \quad (6)$$

To simplify the conversion, τ is calculated by assuming that nanoparticles are monodispersed spheres with all their surfaces exposed:

$$\tau = \frac{6m\eta}{\rho d} \quad (7)$$

where m is the total mass of LDO-Ru-FCC, η is the mass percentage of Ru in LDO-Ru-FCC, and ρ is the density of Ru.[60] Obviously, this assumption overestimates τ and thus underestimates TOF because not all of the surface of a catalyst nanoparticle is exposed when it is fixed on a support. Nonetheless, for the experiment shown in Figure 4a, given m = 3.89 mg, η = 2.6(±0.1)%, ρ = 12.1 g cm^{-3}, and d = 2.0(±0.4) nm, we have τ = 0.025(±0.005) m^2. Together with the value of k_0, we estimate TOF = 0.84(±0.18) mol-H_2 m^{-2}-Ru h^{-1} for 2 nm Ru-FCC nanoparticles at 25 °C.

To obtain A and E_a for Ru-catalyzed NH_3BH_3 hydrolysis, k_0 and TOF are estimated from experiments performed at six different temperatures between 7 and 50 °C. As shown in Figure 4b, the relationship between ln k_0 and $1/T$ conforms to the Arrhenius equation. Least-squares regression to eq 1 gives A = 1045(±302) mol-H_2 m^{-2}-Ru h^{-1} and E_a = 17.7(±0.7) kJ mol^{-1} for 2 nm Ru-FCC nanoparticles.

When the size of the Ru nanoparticles changes, both A and E_a are found to vary systematically. The nanoparticle size is adjusted by changing the concentration of $RuCl_3$ in the solution used to prepare LDO-Ru-FCC. By varying the $RuCl_3$ concentration from 80 to 640 mg L^{-1}, we can increase the mass percentage of Ru from η = 1.2(±0.1) to 8.8(±0.2)%. Accordingly, the mean value of nanoparticle diameter d increases from 2.0(±0.4) to 3.8(±0.5) nm (see Figure S1 in the Supporting Information for diameter histograms), as shown in Figure 5a. As shown in Figure 5b,c, both ln A and E_a increase linearly with the mean value of d (cf. Figure S2 in the Supporting Information), indicating a linear correlation between ln A and E_a as illustrated in Figure 5d. The values of ln A and E_a range from 6.95(±0.29) to 35.8(±2.4) and from

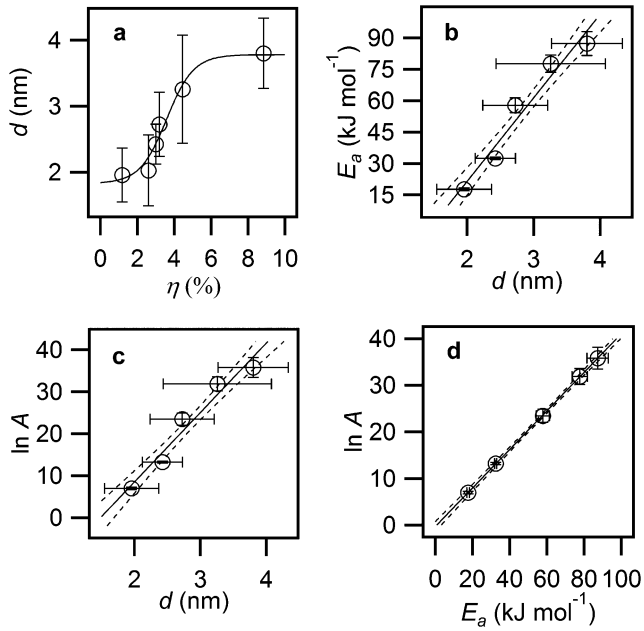

Figure 5. Tuning the catalytic performance of layered double oxide (LDO) supported face-centered cubic (FCC) packed ruthenium (Ru) nanoparticles by adjusting nanoparticle size. (a) Correlation of the nanoparticle diameter d with the mass percentage η of Ru in LDO-Ru; (b) correlation between the activation energy E_a and d; (c) correlation between the logarithm of the Arrhenius pre-exponential factor A (ln A) and d; (d) correlation of ln A and E_a, used to estimate the isokinetic temperature according to eq 3. Solid curves are least-squares regressions ((a), sigmoid; (b)−(d), linear). Dashed curves bracket 95% confidence bands. Error bars for d in (a), (b), and (c) represent one standard deviation range of the corresponding values. All the other error bars represent standard errors.

DOI: 10.1021/cs5019524
ACS Catal. 2015, 5, 1726−1735

17.7(±0.7) to 87.3(±5.8) kJ mol^{-1}, respectively. While the dependence of ln A on d is not normally reported, the dependence of E_a on d for Ru-FCC in ammonia borane hydrolysis is consistent with similar relationships for Pt nanoparticles in ethane hydrogenolysis (E_a = 45−75 kJ mol^{-1} with d = 2−4 nm)[49] and cyclohexene dehydrogenation (E_a = 8−46 kJ mol^{-1} with d = 2−4 nm).[47] The wide ranges of ln A and E_a measured for Ru-catalyzed NH_3BH_3 hydrolysis suggest that the observed correlation between them is unlikely due to experimental or statistical errors but rather originated from the compensation effect.[61−63]

According to eq 3, the least-squares regression between ln A and E_a gives T_i = 290.6(±1.6) K = 17.5(±1.6) °C and TOF$_i$ = 0.72(±0.10) mol-H_2 m^{-2}-Ru h^{-1}. T_i is slightly lower than the value of 20(±11) °C estimated from literature data, whereas TOF$_i$ is much greater than the literature-estimated value of 0.11(±0.08) mol-H_2 m^{-2}-catalyst h^{-1} because Ru is a much better catalyst than other transition metals.[16−41] TOF$_i$ is the TOF ceiling for $T < T_i$, the TOF floor for $T > T_i$, and the invariant TOF value at $T = T_i$, as shown in Figure 6. To

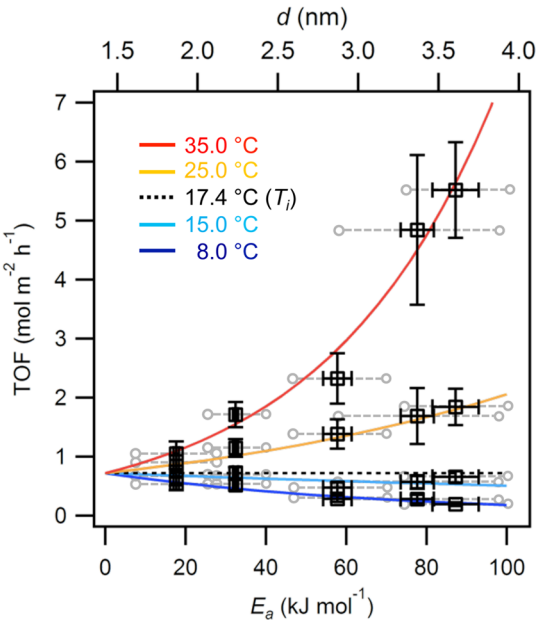

Figure 6. Selection of layered double oxide (LDO) supported Ru-FCC nanoparticles for performing ammonia borane hydrolysis above and below the isokinetic temperature (T_i) according to the particle diameter d (with circle-capped error bars) and the corresponding activation energy E_a (with line-capped error bars). TOF denotes turnover frequency. Error bars represent standard errors.

maximize TOF for $T < T_i$, a catalyst with the lowest E_a should be used. Among all the catalysts prepared in this study, 2 nm Ru-FCC nanoparticles have the lowest E_a of 17.7 kJ mol^{-1}. At 15 °C, the low-activation sample gives TOF = 0.65(±0.14) mol m^{-2} h^{-1}, more than 90% of the theoretical maximum of TOF$_i$. For $T > T_i$, TOF is maximized by using 3.8 nm Ru-FCC nanoparticles having the highest E_a value of 87.3 kJ mol^{-1}. The resulting TOF is 1.8(±0.3) mol m^{-2} h^{-1} at 25 °C, surpassing the highest TOF reported so far for Ru by 81%.[16] Recently, suspended palladium−rhodium (Pd−Rh) nanoparticles protected by poly(*N*-vinyl-2-pyrrolidone) (PVP) has been reported, achieving a TOF of 3.8 mol m^{-2} h^{-1} at 25 °C.[64] Taking into consideration that Ru-FCC nanoparticles affixed on LDO lose part of their surface area due to support blockage (i.e., 53%), the catalytic activity of LDO-Ru-FCC is on par with suspended Pd−Rh nanoparticles on the per-unit-surface-area basis.

In comparison to LDO-Ru-FCC, the size of Ru-HCP nanoparticles formed by directly reducing dissolved Ru^{3+} is insensitive to the $RuCl_3$ concentration, giving a relatively constant diameter of 2.1(±0.4) nm for weight percentages between 1 and 10%. These samples also show an invariant activation energy of E_a = 50.2(±3.5) kJ mol^{-1}. As a result, tuning TOF by adjusting nanoparticle size and activation energy is not possible using Ru-HCP produced by this method.

The use of LDO nanodisks as support for Ru-FCC permits further functionalization of the integrated catalyst without compromising its catalytic activity. We have functionalized LDO with Co nanoparticles before the loading of Ru^{3+}, thereby forming both Co and Ru nanoparticles on LDO (Co-LDO-Ru) after reduction. As shown in Figure 7a, Co and Ru

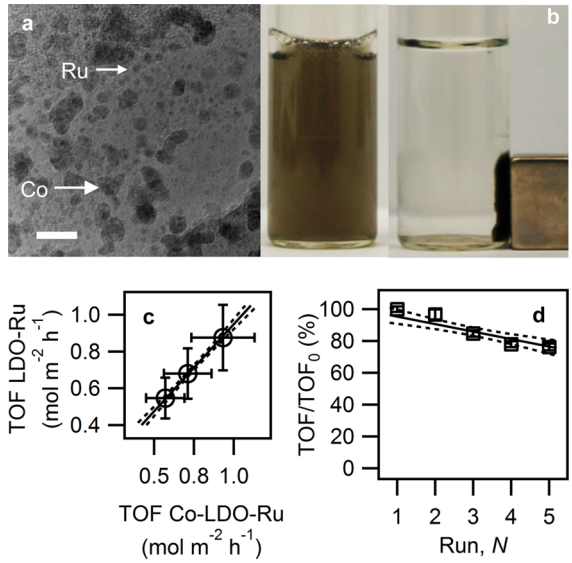

Figure 7. Performance of Ru-FCC supported by layered double oxide (LDO) containing cobalt (Co): (a) coexistence of Ru and Co nanoparticles on LDO; (b) magnetism provided by Co for rapid separation; (c) comparable turnover frequencies (TOFs) of LDO-Ru with and without Co (slope, 0.95(±0.01); R^2 = 0.997); (d) reduction of TOF after repeated use in comparison to the TOF of a pristine sample (TOF$_0$). Dashed curves bracket 95% confidence bands. Error bars represent standard errors. Scale bar: (a), 10 nm.

nanoparticles are separated from one another on LDO. The addition of Co renders magnetism to the catalyst, as shown in Figure 7b, offering the ability to rapidly separate Ru from the exhausted fuel solution. Fresh Co-LDO-Ru shows virtually identical TOF as LDO-Ru containing the same amount of Ru, as illustrated in Figure 7c. Using Co-LDO-Ru, the reuse of Ru-FCC is evaluated. As shown in Figure 7d, TOF reduces by 25.7(±0.3)% after five cycles of reaction, comparable to or better than the performances of most supported Ru nanoparticles. For example (Table S3 in the Supporting Information), the five-cycle TOF reduction is 22% for Ru−Ni core−shell particles supported on graphene,[65] 36% for Ru supported on graphene,[23] 49% for Ru−Co core−shell particles supported on graphene,[66] 58% for Ru supported on carbon black,[20] and 73% for Ru supported on carbon nanotubes.[16] A potential cause of TOF deterioration is the aggregation of Ru

DOI: 10.1021/cs5019524
ACS Catal. 2015, 5, 1726−1735

nanoparticles during the reaction, which can be greatly alleviated by embedding Ru nanoparticles into supports such as hydroxyapatite (8% reduction in five cycles)[27] and zeolite (15% reduction in five cycles).[67] We are in the process of developing a synthesis technique that will permit the embedment of Ru−FCC nanoparticles into LDO nanodisks while still allowing the adjustment of nanoparticle size.

DISCUSSION

Using Ru-FCC nanoparticles supported on LDO, we have shown that both the activation energy and the Arrhenius pre-exponential factor of catalytic ammonia borane hydrolysis increases with nanoparticle diameter for d = 2−3.8 nm according to the compensation effect, giving an isokinetic temperature of 17.5 °C. In this section, we discuss the mechanisms of Ru-FCC formation on the LDO surface and the origin of the compensation effect.

Formation of Ru-FCC on LDO Surface. Ru nanoparticles supported by LDO nanodisks have an FCC structure (Figure 3a−c), different from the HCP Ru nanoparticles formed in solution (Figure 3d−f). HCP is the stable phase for bulk materials,[55,68] indicating a reduction of volumetric Gibbs free energy greater than that for FCC: $-\Delta G_{HCP} > -\Delta G_{FCC}$ ($\Delta G < 0$). According to the classical nucleation theory,[69] Ru nuclei must overcome the interfacial energy associated with surface tension γ before they can grow into nanoparticles spontaneously. The transition between the unsuccessful nucleation and the spontaneous growth happens for nuclei having a diameter greater than a critical value:[69]

$$\lambda = \frac{-4\gamma}{\Delta G} \tag{7}$$

According to eq 7, the preferred formation of HCP nanoparticles over FCC nanoparticles in solution can be attributed to $\lambda_{HCP} < \lambda_{FCC}$ under the assumption of $\gamma_{HCP} \approx \gamma_{FCC}$. This condition ensures that HCP nuclei outcompetes FCC nuclei in solution to grow into nanoparticles.

The extended immersion of LDO into the $RuCl_3$ solution before reduction (Figure 2a) creates strong bonding between Ru^{3+} and LDO, likely formed by the exchange of Ru^{3+} with Al^{3+} in LDO. According to the spinel structure of LDO,[70] each Al^{3+} coordinates with six oxygen atoms at a bond length of 0.19 nm,[71] comparable to the Ru−O bond length of 0.21 nm found with six-coordinated Ru^{3+}.[72] The strong bonding between Ru^{3+} and LDO suggests that, when a nucleus is formed, the surface tension (a result of weak or no affinity between the two phases across an interface) is low, at least on the supported side of the nucleus. The reduction of γ_{FCC} thus leads to a reduction of λ_{FCC}, reversing the preference between FCC and HCP in nanoparticle formation: $\lambda_{FCC} < \lambda_{HCP}$. This mechanism is consistent with previous reports that Ru-FCC nanoparticles can also be synthesized by using the tension-reducing stabilizer PVP[73] and the tension-reducing solvent ethanol.[17] Similar phase-selective synthesis via surface tension adjustment has been performed successfully for iron,[74,75] cobalt,[56] and other types of nanoparticles.[76]

An important consequence of selecting an energetically less favored bulk phase by surface tension adjustment is that the resulting particles are only stable in the nanometer range. In our experiments, the diameter of Ru-FCC nanoparticles increases with the increase of Ru mass percentage rapidly from d = 2 to 3 nm, after which the increasing trend plateaus near d = 3.8 nm (Figure 5a). This indicates that, at d = 3.8 nm, γ_{FCC} is again dominated by the surface tension between the nanoparticle and solvent while the tension-reducing effect of LDO has diminished. Further growth of the nanoparticle would require a phase transition from FCC to HCP, which is not possible without an input of energy.[73]

Origin of the Compensation Effect. Whether an observed linearity between ln A and E_a is evidence of the compensation effect in heterogeneous catalysis has been debated. On one hand, mathematical derivations show that the linearity can arise from errors from measurements and analyses.[61,62] On the other hand, the presence and prevalence of such errors in experiments remain to be demonstrated.[63] In this study, we have taken precautions in measurements and analyses to minimize the potential hazard of systematic errors (cf. Figure 4a and Table S2 in the Supporting Information) as recommended in the literature.[77] The ln A−E_a linearity observed in Ru-catalyzed ammonia borane hydrolysis is, therefore, taken as evidence of the compensation effect according to generally accepted standards.[63]

Ru-catalyzed ammonia borane hydrolysis likely follows a mechanism similar to that of metal-catalyzed borohydride (BH_4^-) hydrolysis:[11,78]

$$NH_3BH_3 + 2Ru \rightleftarrows NH_3BH_2Ru + RuH \tag{8}$$

$$NH_3BH_2Ru + H_2O \rightarrow NH_3BH_2OH + RuH \tag{9}$$

$$NH_3BH_2OH + 2Ru \rightarrow NH_3BH(OH)Ru + RuH \tag{10}$$

$$NH_3BH(OH)Ru + H_2O \rightarrow NH_3BH(OH)_2 + RuH \tag{11}$$

$$NH_3BH(OH)_2 + 2Ru \rightarrow NH_3B(OH)_2Ru + RuH \tag{12}$$

$$NH_3B(OH)_2Ru + H_2O \rightarrow NH_3B(OH)_3 + RuH \tag{13}$$

$$RuH + RuH \rightarrow 2Ru + H_2 \tag{14}$$

and

$$NH_3B(OH)_3 \rightarrow NH_4^+ + BO_2^- + H_2O \tag{15}$$

The rate of the overall reaction is limited by the rate of reaction 9 involving the breaking of the O−H bond of water.[79] By applying the transition state theory to the rate-limiting reaction, TOF of the overall reaction can be described by the Eyring equation:[80]

$$\mathrm{TOF} = \mathrm{TOF_i}\exp\left(\frac{\Delta S^{\mathrm{T}} + \Delta S^{\mathrm{C}}}{R}\right)\exp\left(-\frac{\Delta H^{\ddagger}}{RT}\right) \tag{16}$$

where ΔS^T is the reduction of thermal entropy, ΔS^C is the reduction of configuration entropy, and $\Delta H^{\ddagger}$ is the enthalpy of activation for reaction 9. $\Delta H^{\ddagger}$ is related to E_a by the Temkin equation:[81]

$$E_a = \Delta H^{\ddagger} + \sum n_i \Delta H_i \tag{17}$$

where ΔH_i is the adsorption enthalpies of reactant i and n_i is its reaction order. For zero-order reactions with n_i = 0, we have

$$E_a = \Delta H^{\ddagger} \tag{18}$$

The ammonia borane hydrolysis is a zeroth-order reaction, as shown by fitting Figure 4a to eq 5 as well as further validation made by experiments conducted with different NH_3BH_3 initial concentrations (Figure S3 in the Supporting Information);

DOI: 10.1021/cs5019524
ACS Catal. 2015, 5, 1726−1735

therefore, eq 18 applies to the hydrolysis reaction. By comparing eqs 16 and 18 with eq 2, we obtain

$$\ln \frac{A}{\mathrm{TOF_i}} = \frac{\Delta S^{\mathrm{T}}}{R} + \frac{\Delta S^{\mathrm{C}}}{R} \tag{19}$$

Since ΔS^{T} quantifies the loss of translational freedom of water upon adsorption, it remains relatively constant for different catalysts.[6,80] Hence, ln A and E_a are regulated by ΔS^{C} and $\Delta H^{\ddagger}$, respectively.

We can estimate ΔS^{C} and $\Delta H^{\ddagger}$ by considering the contributions of different types of atoms on the surfaces of nanocrystalline catalysts. We separate the surface atoms into two different groups:[82−84] (1) corner and edge (c/e) and (2) terrace (t) atoms. Because ΔS^{C} quantifies the number of configurations of empty sites,[80] it has a greater value on two-dimensional terraces than one-dimensional edges (including corners): $\Delta S_{\mathrm{t}}^{\mathrm{C}} > \Delta S_{\mathrm{c/e}}^{\mathrm{C}}$. In comparison to edge and corner atoms that have more unsatisfied bonds, terrace atoms are better coordinated, bind reactants more loosely, and thus result in less stable intermediates with a higher enthalpy:[85,86] $\Delta H_{\mathrm{t}}^{\ddagger} > \Delta H_{\mathrm{c/e}}^{\ddagger}$. Using these parameters, we can rewrite eqs 18 and 19 using $\Delta S^{\mathrm{C}} = (1 - f)\Delta S_{\mathrm{t}}^{\mathrm{C}} + f\Delta S_{\mathrm{c/e}}^{\mathrm{C}}$ and $\Delta H^{\ddagger} = (1 - f)\Delta H_{\mathrm{t}}^{\ddagger} + f\Delta H_{\mathrm{c/e}}^{\ddagger}$:

$$\ln \frac{A}{\mathrm{TOF_i}} = \frac{\Delta S^{\mathrm{T}} + \Delta S_{\mathrm{t}}^{\mathrm{C}}}{R} - \frac{\Delta S_{\mathrm{t}}^{\mathrm{C}} - \Delta S_{\mathrm{c/e}}^{\mathrm{C}}}{R} f \tag{20}$$

and

$$E_{\mathrm{a}} = \Delta H_{\mathrm{t}}^{\ddagger} - (\Delta H_{\mathrm{t}}^{\ddagger} - \Delta H_{\mathrm{c/e}}^{\ddagger}) f \tag{21}$$

where f is the fraction of edge and corner atoms on the nanoparticle surface. According to eqs 20 and 21, ln A and E_a are positively correlated following the changes of $\Delta S_{\mathrm{t}}^{\mathrm{C}} - \Delta S_{\mathrm{c/e}}^{\mathrm{C}}$ and $\Delta H_{\mathrm{t}}^{\ddagger} - \Delta H_{\mathrm{c/e}}^{\ddagger}$ with f being the scaling factor for both ln A and E_a.

Ru-FCC nanoparticles supported on LDO nanodisks have truncated octahedral shapes (Figure 3a−c). As shown in Figure 8a, a truncated octahedron has 14 facets, including eight {111} facets and six {100} facets with 24 edges and 12 corners. The fraction of edge and corner atoms with respect to the total number of surface atoms can be computed using the equation (see Note S1 in the Supporting Information for derivation):

$$f = \frac{0.89d - 0.40}{d^2 - 0.52d + 0.096} \tag{22}$$

where d is expressed in nanometers. As d increases from 2 to 3.8 nm, f decreases from 46 to 24%. As shown in Figure 8b,c, the decrease of f with d correlates with the decreases of ln A and E_a, as depicted by eqs 20 and 21. According to these equations, least-squares regressions give $\Delta S^{\mathrm{T}} + \Delta S_{\mathrm{t}}^{\mathrm{C}} = 571(\pm 45)$ J mol^{-1} K^{-1}, $\Delta S_{\mathrm{t}}^{\mathrm{C}} - \Delta S_{\mathrm{c/e}}^{\mathrm{C}} = 1139(\pm 131)$ J mol^{-1} K^{-1}, $\Delta H_{\mathrm{t}}^{\ddagger} = 165(\pm 14)$ kJ mol^{-1}, and $\Delta H_{\mathrm{t}}^{\ddagger} - \Delta H_{\mathrm{c/e}}^{\ddagger} = 330(\pm 40)$ kJ mol^{-1}. The positive value of $\Delta H_{\mathrm{t}}^{\ddagger} - \Delta H_{\mathrm{c/e}}^{\ddagger}$ estimated from regression indicates that H_2O can interact with NH_3BH_2Ru more readily when NH_3BH_2Ru is located at corners and edges, instead of terraces, of a Ru nanoparticle. Density functional theory (DFT) calculations suggest that molecules such as CH_xO (x = 1−3) and CH_x (x = 1−4) favor c/e sites over t sites on Pt and Pd by 20−80 kJ mol^{-1}.[85,86] To account for a large difference of 330 kJ mol^{-1}, we propose that the orientation by which H_2O approaches NH_3BH_2Ru on the terrace should play an important role in determining the enthalpy of the transition state.[87,88] The number of neighboring atoms is greatly reduced at edge and corner sites, thereby leading to the reduction of energy requirement for interaction.

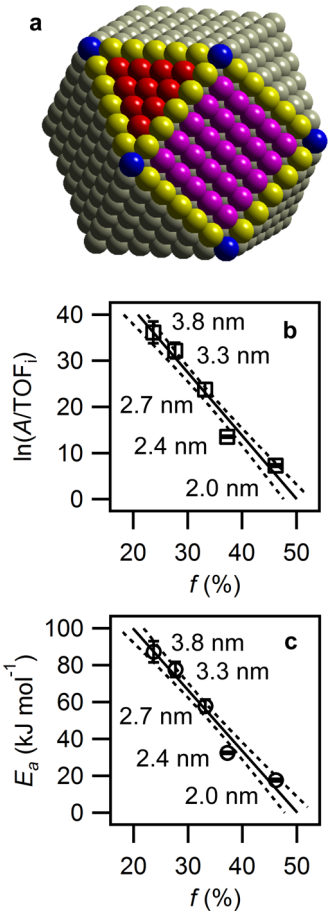

Figure 8. Dependences of the logarithm of the Arrhenius pre-exponential factor (ln A) and the activation energy (E_a) on the fraction (f) of edge and corner atoms of Ru-FCC nanoparticles: (a) truncated octahedron model for a Ru-FCC nanoparticle, showing one {111} facet (red), one {100} facet (purple), and their adjacent edges (yellow) and corners (blue); (b, c) correlations of ln A and E_a with f. The values given at each data point are mean diameters of the nanoparticles. The solid lines are least-squares regressions. The dashed lines bracket 95% confidence bands. Error bars represent standard errors.

CONCLUSIONS

Using Ru-FCC nanoparticles supported on LDO nanodisks, we have shown that the turnover frequency of NH_3BH_3 hydrolysis can be maximized for operations below and above the isokinetic temperature by simply tuning the nanoparticle size, providing a viable strategy to match catalyst design with operational conditions. Hydrogen stored in ammonia borane can be released by either catalytic solvolysis[89,90] or thermal decomposition[91,92] reactions. Thermal decomposition is often considered preferable because solid NH_3BH_3 instead of saturated NH_3BH_3 solution is used to maximize the storage capacity. The thermal decomposition of pure NH_3BH_3 requires an operational temperature of approximately 150 °C to yield a reasonable hydrogen generation rate.[93,94] At high temperatures, a significant amount of NH_3BH_3 can decompose to form byproducts such as borazine, ammonia, and diborane, a process that not only lowers conversion efficiency but also contam-

DOI: 10.1021/cs5019524
ACS Catal. 2015, 5, 1726−1735

inates the fuel stream.[95] To lower the operational temperature of thermal decomposition, NH_3BH_3 is mixed with catalysts at high catalyst to fuel ratios, which reduce the weight-based storage capacity to levels similar to that of an saturated NH_3BH_3 aqueous solution.[96] In comparison, the catalytic hydrolysis of ammonia borane can be operated at ambient temperatures without concerns of the aforementioned by-products.

MATERIALS AND METHODS

Reagent-grade chemicals were purchased from Sigma-Aldrich unless otherwise specified. Deionized (DI) water was produced using a Millipore system on site.

Preparation of LDO Nanodisks. LDO was prepared using a hydrothermal method.[70] Briefly, synthesis was performed using 100 mL of an aqueous solution of urea ($CO(NH_2)_2$; 100 mM), aluminum nitrate ($Al(NO_3)_3$; 50 mM), and magnesium nitrate ($Mg(NO_3)_2$; 50 mM). A 100 mL portion of the solution was placed in a sealed autoclave reactor, which was then heated to 100 °C and maintained at this temperature for 12 h. The solid product of the hydrothermal synthesis was collected by centrifugation, washed with DI water, and freeze-dried (Labconco Freezone 4.5). The dried powder was heated to 600 °C in a sealed quartz tube under argon protection. After the temperature had been stable for 5 min, hydrogen was injected into the tubing at 50 sccm for 5 min to produce LDO nanodisks. To add cobalt nanoparticles on LDO, half of the $Mg(NO_3)_2$ was replaced by cobalt nitrate ($Co(NO_3)_2$) in the hydrothermal synthesis.

Fixation of Ruthenium Nanoparticles on LDO Nanodisks. A stock solution of 1000 ppm Ru was prepared by dissolving 53 mg of $RuCl_3$ hydrate (35−40% Ru by weight, ACROS Organics) into 20 mL of DI water. The synthesis of LDO-Ru-FCC consists of two major steps, as illustrated in Figure 2a. First, 20 mg LDO and an aliquot of $RuCl_3$ stock solution (0.6, 1.2, 1.8, 2.4, 3.0, or 4.8 mL) were mixed with DI water to a total volume of 7.5 mL. The mixture was sonicated for 10 min and mixed on a shaking table for 24 h. LDO nanodisks adsorbed with Ru^{3+} were collected by centrifugation, washed three times with DI water, and freeze-dried. Second, 4 mg of the LDO dry powder were redispersed in 10 mL of DI water and sonicated for 10 min. Ru nanoparticles were then formed when NH_3BH_3 was added to the solution to initiate the hydrolysis reaction (see below). To synthesize Ru-HCP, 4 mg of the LDO dry powder and 0.1 mL of the $RuCl_3$ stock solution were mixed with 10 mL of DI water with sonication for 2 min. Ammonia borane was then added to reduce Ru^{3+} and also initiate hydrolysis to generate hydrogen.

Material Characterization. LDO, Co-LDO, and Ru nanoparticles supported by them were characterized using atomic force microscopy (Park Systems XE-70) and transmission electron microscopy (FEI Titan 80−300). The ruthenium contents were determined after digesting the samples before reduction with 70% nitric acid for 12 h at 80 °C. The concentration of Ru in the digestion solution was measured using ion-coupled plasma optical emission spectroscopy (PerkinElmer Optima 2000).

Evaluation of Catalytic Performance. Performances of LDO-Ru-FCC and LDO-Ru-HCP were evaluated by measuring the volume of accumulated H_2 released from NH_3BH_3 hydrolysis using a water-filled gas buret.[89] This analytical method was validated by confirming that only a trace amount of ammonia existed in the produced gas. Ammonia was captured by passing the gas through 20 mL of an HCl solution (1 mM). The amount of ammonia was determined colorimetrically from the difference between the original proton concentration and the remaining concentration, both of which were titrated with a standard NaOH solution (2.5 mM) using phenolphthalein as an indicator.[23,34]

To initiate the reaction at 25 °C, 10 mL of DI water containing well-dispersed catalyst precursors was transferred into a 25 mL flask containing a Teflon-coated stir bar. The flask was placed in a water-bath stirrer set at a stirring rate of 1000 rpm. After the solution in the flask reached the preset temperature, 31.8 mg of ammonia borane was added into the flask. Immediately, the water-filled gas buret was connected to the flask. The volume of accumulated H_2 in the buret was read periodically as gas replaced water. For reactions performed at temperatures other than 25 °C (between 7 and 50 °C), 0.1 mg of LDO-Ru-FCC was formed at 25 °C by adding 10 mL of a 0.01 M NH_3BH_3 solution before the temperature was adjusted to the experimental value. The purpose of this protocol was to prevent the potential influence of temperature on nanoparticle size.[97]

The reuse of Ru-FCC was tested using Co-LDO as support at 25 °C. After the first run was complete, the catalyst was separated from the solution using a block magnet (K&J Magnetics BX0X0C). After the solution was decanted, 10 mL of a 0.1 M NH_3BH_3 solution was placed in the flask to start another run of the experiment.

ASSOCIATED CONTENT

Supporting Information

The following file is available free of charge on the ACS Publications website at DOI: 10.1021/cs5019524.

Table S1 (literature data used to plot Figure 1), Table S2 (selection of data for performing the linear regression in Figure 4a), Table S3 (reduction in catalytic activity of supported Ru nanoparticles reported in the literature), Figure S1 (histograms of the nominal diameters of Ru-FCC nanoparticles supported on layered double oxide nanodisks), Figure S2 (correlation of the turnover frequency with temperature for Ru-FCC with five different sizes), Figure S3 (independence of ammonia borane hydrolysis on the initial concentration), and Note S1 (fraction of atoms located at edges and corners in a truncated octahedron) (PDF)

AUTHOR INFORMATION

Corresponding Author

*E-mail for C.N.: chongzheng.na@gmail.com.

Notes

The authors declare no competing financial interest.

ACKNOWLEDGMENTS

We thank the DOE Office of Nuclear Energy's Nuclear Energy University Programs, the National Science Foundation's Environmental Engineering Program, and the University of Notre Dame Sustainable Energy Initiative for financial support. H.M. also acknowledges support from the Bayer Predoctoral Research Fellowship, provided by the Notre Dame Center for Environmental Science and Technology.

DOI: 10.1021/cs5019524
ACS Catal. 2015, 5, 1726−1735

REFERENCES

(1) Masel, R. I. *Principles of Adsorption and Reaction on Solid Surfaces*; Wiley: New York, 1996; p 482−610.
(2) Lopez, N.; Janssens, T. V. W.; Clausen, B. S.; Xu, Y.; Mavrikakis, M.; Bligaard, T.; Nørskov, J. K. *J. Catal.* **2004**, *223*, 232−235.
(3) Constable, F. H. *Proc. R. Soc. A* **1925**, *108*, 355−378.
(4) Palmer, W. G.; Constable, F. H. *Proc. R. Soc. A* **1924**, *106*, 251−268.
(5) Bond, G. C.; Keane, M. A.; Kral, H.; Lercher, J. A. *Catal. Rev.* **2000**, *42*, 323−383.
(6) Bligaard, T.; Honkala, K.; Logadottir, A.; Nørskov, J. K.; Dahl, S.; Jacobsen, C. J. H. *J. Phys. Chem. B* **2003**, *107*, 9325−9331.
(7) Kozuch, S.; Shaik, S. *J. Am. Chem. Soc.* **2006**, *128*, 3355−3365.
(8) Kozuch, S.; Martin, J. M. L. *ACS Catal.* **2012**, *2*, 2787−2794.
(9) Linert, W. *Chem. Phys.* **1989**, *129*, 381−393.
(10) Marder, T. B. *Angew. Chem., Int. Ed.* **2007**, *46*, 8116−8118.
(11) Demirci, U. B.; Miele, P. *Energy Environ. Sci.* **2009**, *2*, 627−637.
(12) Liu, C.; Li, F.; Ma, L. P.; Cheng, H. M. *Adv. Mater.* **2010**, *22*, E28−+.
(13) Heinzel, A.; Hebling, C.; Muller, M.; Zedda, M.; Muller, C. *J. Power Sources* **2002**, *105*, 250−255.
(14) Dyer, C. K. *J. Power Sources* **2002**, *106*, 31−34.
(15) Patil, A. S.; Dubois, T. G.; Sifer, N.; Bostic, E.; Gardner, K.; Quah, M.; Bolton, C. *J. Power Sources* **2004**, *136*, 220−225.
(16) Akbayrak, S.; Ozkar, S. *ACS Appl. Mater. Interfaces* **2012**, *4*, 6302−6310.
(17) Abo-Hamed, E. K.; Pennycook, T.; Vaynzof, Y.; Toprakcioglu, C.; Koutsioubas, A.; Scherman, O. A. *Small* **2014**, *10*, 3145−3152.
(18) Metin, Ö.; Şahin, Ş.; Özkar, S. *Int. J. Hydrogen Energy* **2009**, *34*, 6304−6313.
(19) Durap, F.; Zahmakiran, M.; Ozkar, S. *Int. J. Hydrogen Energy* **2009**, *34*, 7223−7230.
(20) Liang, H. Y.; Chen, G. Z.; Desinan, S.; Rosei, R.; Rosei, F.; Ma, D. L. *Int. J. Hydrogen Energy* **2012**, *37*, 17921−17927.
(21) Caliskan, S.; Zahmakiran, M.; Durap, F.; Ozkar, S. *Dalton Trans.* **2012**, *41*, 4976−4984.
(22) Can, H.; Metin, Ö. *Appl. Catal., B* **2012**, *125*, 304−310.
(23) Cao, N.; Luo, W.; Cheng, G. Z. *Int. J. Hydrogen Energy* **2013**, *38*, 11964−11972.
(24) Yao, Q.; Shi, W.; Feng, G.; Lu, Z.-H.; Zhang, X.; Tao, D.; Kong, D.; Chen, X. *J. Power Sources* **2014**, *257*, 293−299.
(25) Akbayrak, S.; Tanyıldızı, S.; Morkan, İ.; Özkar, S. *Int. J. Hydrogen Energy* **2014**, *39*, 9628−9637.
(26) Akbayrak, S.; Ozkar, S. *Dalton Trans.* **2014**, *43*, 1797−1805.
(27) Akbayrak, S.; Erdek, P.; Ozkar, S. *Appl. Catal., B* **2013**, *142*, 187−195.
(28) Chen, W.; Ji, J.; Duan, X.; Qian, G.; Li, P.; Zhou, X.; Chen, D.; Yuan, W. *Chem. Commun.* **2014**, *50*, 2142−2144.
(29) Chandra, M.; Xu, Q. *J. Power Sources* **2007**, *168*, 135−142.
(30) Karatas, Y.; Yurderi, M.; Gulcan, M.; Zahmakiran, M.; Kaya, M. *J. Nanopart. Res.* **2014**, *16*, 1−12.
(31) Akbayrak, S.; Kaya, M.; Volkan, M.; Özkar, S. *Appl. Catal., B* **2014**, *147*, 387−393.
(32) Xi, P.; Chen, F.; Xie, G.; Ma, C.; Liu, H.; Shao, C.; Wang, J.; Xu, Z.; Xu, X.; Zeng, Z. *Nanoscale* **2012**, *4*, 5597−5601.
(33) Kılıç, B.; Şencanlı, S.; Metin, Ö. *J. Mol. Catal. A: Chem.* **2012**, *361−362*, 104−110.
(34) Metin, Ö.; Mazumder, V.; Özkar, S.; Sun, S. *J. Am. Chem. Soc.* **2010**, *132*, 1468−1469.
(35) Metin, Ö.; Özkar, S.; Sun, S. *Nano Res.* **2010**, *3*, 676−684.
(36) Zhou, L.; Zhang, T.; Tao, Z.; Chen, J. *Nano Res.* **2014**, *7*, 774−781.
(37) Hu, J.; Chen, Z.; Li, M.; Zhou, X.; Lu, H. *ACS Appl. Mater. Interfaces* **2014**, *6*, 13191−13200.
(38) Rakap, M.; Özkar, S. *Catal. Today* **2012**, *183*, 17−25.
(39) Xu, Q.; Chandra, M. *J. Alloys Compd.* **2007**, *446−447*, 729−732.
(40) Metin, Ö.; Özkar, S. *Energy Fuels* **2009**, *23*, 3517−3526.
(41) Dinç, M.; Metin, Ö.; Özkar, S. *Catal. Today* **2012**, *183*, 10−16.
(42) Yan, J.-M.; Zhang, X.-B.; Akita, T.; Haruta, M.; Xu, Q. *J. Am. Chem. Soc.* **2010**, *132*, 5326−5327.
(43) Jiang, H.-L.; Umegaki, T.; Akita, T.; Zhang, X.-B.; Haruta, M.; Xu, Q. *Chem.—Eur. J.* **2010**, *16*, 3132−3137.
(44) Chen, G.; Desinan, S.; Rosei, R.; Rosei, F.; Ma, D. *Chem. Eur. J.* **2012**, *18*, 7925−7930.
(45) Rakap, M. *Appl. Catal., A* **2014**, *478*, 15−20.
(46) Sun, D.; Mazumder, V.; Metin, Ö.; Sun, S. *ACS Nano* **2011**, *5*, 6458−6464.
(47) Somorjai, G. A.; Park, J. Y. *Top. Catal.* **2008**, *49*, 126−135.
(48) Johnson, J. A.; Makis, J. J.; Marvin, K. A.; Rodenbusch, S. E.; Stevenson, K. J. *J. Phys. Chem. C* **2013**, *117*, 22644−22651.
(49) Song, H.; Rioux, R. M.; Hoefelmeyer, J. D.; Komor, R.; Niesz, K.; Grass, M.; Yang, P.; Somorjai, G. A. *J. Am. Chem. Soc.* **2006**, *128*, 3027−3037.
(50) Hou, C.-H.; Huang, J.-F.; Lin, H.-R.; Wang, B.-Y. *J. Taiwan Inst. Chem. E* **2012**, *43*, 473−479.
(51) Tian, G.-L.; Zhao, M.-Q.; Zhang, B.; Zhang, Q.; Zhang, W.; Huang, J.-Q.; Chen, T.-C.; Qian, W.-Z.; Su, D. S.; Wei, F. *J. Mater. Chem. A* **2014**, *2*, 1686−1696.
(52) Fan, G.; Li, F.; Evans, D. G.; Duan, X. *Chem. Soc. Rev.* **2014**, *43*, 7040−7066.
(53) Ma, H.; Wang, H.; Na, C. *Appl. Catal., B* **2015**, *163*, 198−204.
(54) Wyckoff, R. W. G. *Crystal Structures*. 2nd ed.; Interscience: New York, 1963; pp 85−237.
(55) Watanabe, S.; Komine, T.; Kai, T.; Shiiki, K. *J. Magn. Magn. Mater.* **2000**, *220*, 277−284.
(56) Kitakami, O.; Sato, H.; Shimada, Y.; Sato, F.; Tanaka, M. *Phys. Rev. B* **1997**, *56*, 13849−13854.
(57) Moussa, G.; Moury, R.; Demirci, U. B.; Miele, P. *Int. J. Hydrogen Energy* **2013**, *38*, 7888−7895.
(58) Sanyal, U.; Demirci, U. B.; Jagirdar, B. R.; Miele, P. *ChemSusChem* **2011**, *4*, 1731−1739.
(59) Lu, Z. H.; Li, J. P.; Zhu, A. L.; Yao, Q. L.; Huang, W.; Zhou, R. Y.; Zhou, R. F.; Chen, X. S. *Int. J. Hydrogen Energy* **2013**, *38*, 5330−5337.
(60) Lide, D. R. *CRC Handbook of Chemistry and Physics*; CRC Press: New York, 2006; p 130.
(61) Barrie, P. J. *Phys. Chem. Chem. Phys.* **2012**, *14*, 318−326.
(62) Barrie, P. J. *Phys. Chem. Chem. Phys.* **2012**, *14*, 327−336.
(63) Yelon, A.; Sacher, E.; Linert, W. *Phys. Chem. Chem. Phys.* **2012**, *14*, 8232−8234.
(64) Rakap, M. *Appl. Catal., B* **2015**, *163*, 129−134.
(65) Cao, N.; Su, J.; Luo, W.; Cheng, G. Z. *Int. J. Hydrogen Energy* **2014**, *39*, 426−435.
(66) Cao, N.; Su, J.; Luo, W.; Cheng, G. Z. *Catal. Commun.* **2014**, *43*, 47−51.
(67) Zahmakiran, M. *Mater. Sci. Eng. B-Adv.* **2012**, *177*, 606−613.
(68) Saunders, N.; Miodownik, A. P.; Dinsdale, A. T. *Calphad* **1988**, *12*, 351−374.
(69) Fletcher, N. H. *J. Chem. Phys.* **1958**, *29*, 572−576.
(70) Wang, H.; Ma, H.; Zheng, W.; An, D.; Na, C. *ACS Appl. Mater. Interfaces* **2014**, *6*, 9426−9434.
(71) Emel'yanov, V. A.; Virovets, A. V.; Baidina, I. A. *J. Struct. Chem.* **2008**, *49*, 566−569.
(72) Peterson, R. C.; Lager, G. A.; Hitterman, R. L. *Am. Mineral.* **1991**, *76*, 1455−1458.
(73) Kusada, K.; Kobayashi, H.; Yamamoto, T.; Matsumura, S.; Naoya, S.; Sato, K.; Nagaoka, K.; Kubota, Y.; Kitagawa, H. *J. Am. Chem. Soc.* **2013**, *135*, 5493−5496.
(74) Kim, H.; Kaufman, M. J.; Sigmund, W. M.; Jacques, D.; Andrews, R. *J. Mater. Chem.* **2003**, *18*, 1104−1108.
(75) Ling, T.; Xie, L.; Zhu, J.; Yu, H.; Ye, H.; Yu, R.; Cheng, Z.; Liu, L.; Yang, G.; Cheng, Z.; Wang, Y.; Ma, X. *Nano Lett.* **2009**, *9*, 1572−1576.
(76) White, R. J.; Luque, R.; Budarin, V. L.; Clark, J. H.; Macquarrie, D. J. *Chem. Soc. Rev.* **2009**, *38*, 481−494.
(77) Barrie, P. J. *Phys. Chem. Chem. Phys.* **2012**, *14*, 8235−8236.

DOI: 10.1021/cs5019524
ACS Catal. 2015, 5, 1726−1735

(78) Guella, G.; Zanchetta, C.; Patton, B.; Miotello, A. *J. Phys. Chem. B* **2006**, *110*, 17024−17033.
(79) Guella, G.; Patton, B.; Miotello, A. *J. Phys. Chem. C* **2007**, *111*, 18744−18750.
(80) Teschner, D.; Novell-Leruth, G.; Farra, R.; Knop-Gericke, A.; Schlögl, R.; Szentmiklósi, L.; Hevia, M. G.; Soerijanto, H.; Schomäcker, R.; Pérez-Ramírez, J.; López, N. *Nat. Chem.* **2012**, *4*, 739−745.
(81) Bond, G. C.; Hooper, A. D.; Slaa, J. C.; Taylor, A. O. *J. Catal.* **1996**, *163*, 319−327.
(82) Narayanan, R.; El-Sayed, M. A. *Nano Lett.* **2004**, *4*, 1343−1348.
(83) Bratlie, K. M.; Lee, H.; Komvopoulos, K.; Yang, P.; Somorjai, G. A. *Nano Lett.* **2007**, *7*, 3097−3101.
(84) Mahmoud, M. A.; Narayanan, R.; El-Sayed, M. A. *Acc. Chem. Res.* **2013**, *46*, 1795−1805.
(85) Kozlov, S. M.; Cabeza, G. F.; Neyman, K. M. *Chem. Phys. Lett.* **2011**, *506*, 92−97.
(86) Viñes, F.; Lykhach, Y.; Staudt, T.; Lorenz, M. P. A.; Papp, C.; Steinrück, H.-P.; Libuda, J.; Neyman, K. M.; Görling, A. *Chem.—Eur. J.* **2010**, *16*, 6530−6539.
(87) Tamura, M.; Sawabe, K.; Tomishige, K.; Satsuma, A.; Shimizu, K.-i. *ACS Catal.* **2014**, *5*, 20−26.
(88) Rasmussen, A. M. H.; Groves, M. N.; Hammer, B. *ACS Catal.* **2014**, *4*, 1182−1188.
(89) Jiang, H. L.; Xu, Q. *Catal. Today* **2011**, *170*, 56−63.
(90) Graham, T. W.; Tsang, C. W.; Chen, X. H.; Guo, R. W.; Jia, W. L.; Lu, S. M.; Sui-Seng, C.; Ewart, C. B.; Lough, A.; Amoroso, D.; Abdur-Rashid, K. *Angew. Chem., Int. Ed.* **2010**, *49*, 8708−8711.
(91) He, T.; Xiong, Z. T.; Wu, G. T.; Chu, H. L.; Wu, C. Z.; Zhang, T.; Chen, P. *Chem. Mater.* **2009**, *21*, 2315−2318.
(92) Wright, W. R. H.; Berkeley, E. R.; Alden, L. R.; Baker, R. T.; Sneddon, L. G. *Chem. Commun.* **2011**, *47*, 3177−3179.
(93) Stowe, A. C.; Shaw, W. J.; Linehan, J. C.; Schmid, B.; Autrey, T. *Phys. Chem. Chem. Phys.* **2007**, *9*, 1831−1836.
(94) Demirci, U. B.; Bernard, S.; Chiriac, R.; Toche, F.; Miele, P. *J. Power Sources* **2011**, *196*, 279−286.
(95) Tang, Z.; Chen, H.; Chen, X.; Wu, L.; Yu, X. *J. Am. Chem. Soc.* **2012**, *134*, 5464−5467.
(96) Tang, Z.; Chen, X.; Chen, H.; Wu, L.; Yu, X. *Angew. Chem., Int. Ed.* **2013**, *52*, 5832−5835.
(97) Pelzer, K.; Vidoni, O.; Philippot, K.; Chaudret, B.; Collière, V. *Adv. Funct. Mater.* **2003**, *13*, 118−126.

DOI: 10.1021/cs5019524
ACS Catal. 2015, 5, 1726−1735